Properties of $(CuO)_{1-x}(ZnO)_x$ thin films deposited by spray pyrolysis

L. HERISSI[1,2,*], L. HADJERIS[2], M.S. AIDA[3], N. ATTAF[4], S. SIOUANE[1]
[1]*Department of Matter Sciences, Echahid Cheikh Larbi Tebessi University, Tebessa 12000, Algeria*
[2]*LMSSEF, Larbi Ben M'hidi University, Oum El Bouaghi 04000, Algeria*
[3]*Center of Nanotechnology, KAU University, Jeddah 22254, Saudi Arabia*
[4]*Phases Transformation Laboratory (LTPh), UMC Constantine1 University, 25000, Algeria*

The main goal of thiswork is the study of $(CuO)_{1-x}(ZnO)_x$ metal oxide thin films to determine their applicability in optoelectronic devices. For this goal, films with a rough surface and good adhesion to the glass substrates with x = 0, 0.25, 0.50, 0.75 and 1, were deposited by spray pyrolysis technique at 450 °C. Copper (II) chloride dihydrate and zinc acetate dihydrate were used as precursors. Structural, optical, and electrical properties of the films have been studied.The obtained results indicate the formation of CuO and ZnO phases unite together primarily through intra-grain coupling mixed in defined proportions for intermediate compositions and the lattice constants of ZnO increase with the nominal fraction x of Zn. Also, there is an increase in the optical gap energy and electrical conductivity in contrast to the Urbach energy which indicates that the defect density decreases with the mixing of Zn into the host CuO lattice as well as the presence of ZnO phase. Furthermore, it was observed that optical transmittance of the as-deposited films increased with increasing the Znconcentration. Consequently, the optical absorption edge gradually shifted towards shortens wavelength side, resulting in the increase of band gap energy.

(Received November 1, 2024; accepted October 14, 2025)

Keywords: Metal oxide thin films, Spray pyrolysis, Lattice parameters, optical gap energy, Electrical conductivity

1. Introduction

Transition metals have many attracting properties such as copper oxide (CuO) and zinc oxide (ZnO). Their alloys lead to new interesting features which may improve optoelectronic properties [1,2].

CuO is a non-toxic, eco-friendly chemical with a square planar coordination of oxygen and copper in the monoclinic structure [3-6]. In addition to its smart optoelectronic properties as a p-type semiconductor, it has high solar spectrum absorption due to its 1.3-2.1 eV optical gap. CuO has been the subject of many researches which allowed its use in several applications such as photodetectors, gas sensors and photocatalysis [3,7,8]. On the other hand, ZnO is a biocompatible, green properties, inorganic compound, low price semiconductor, non-toxic and cost-effective starting material for generating massive amount of reactive oxygen species and hot charge carriers that scavenge organic pollutants from wastewater [9-11]. ZnO has a large bandgap of 3.37 eV at room temperature, an excellent stability, a high binding energy of 60 meV, and it exhibits good piezoelectric capabilities [2,9,11].

In this context, several authors [11-17] have prepared CuO:Zn and ZnO:Cu thin films by electrodeposition, sol-gel method, solid-state, hydrothermal, co-precipitation, RF magnetron sputtering, DC magnetron sputtering, pulsed laser deposition, aerosol assisted chemical vapor deposition and spray pyrolysis technique. The structural, electrical and optical properties of the films have been characterized. The purpose of this study is to exploit the difference between CuO and ZnO structures and to use their mixture to obtain a material having a high porosity which makes it useful for application as agas sensor [18,19]. For example, the researchers prepared copper doped zinc oxide hence the achieved irregular structure with dimensions varied from 50 to 100 nm [2]. Also, CuO is a p-type material while ZnO is n-type [2], the conductivity type can be easily controlled by changing the nominal fraction x of Zn when depositing $(CuO)_{1-x}(ZnO)_x$ films. The conductivity evolves from p-type when x = 0 to n-type if x = 1. Therefore, the creation of $(CuO)_{1-x}(ZnO)_x$ provides new properties and therefore enhanced performances [2].

The aim of the present work is the preparation, by spray pyrolysis technique, of $(CuO)_{1-x}(ZnO)_x$ thin films and the study of the influence of the x values on their structural, optical, and electrical properties. The deposition method was chosen for its many advantages, namely: simplicity, low-cost setup, ability to deposit large areas of thin films, a control over material composition, vacuum-less equipment and being the most versatile technology for coating films directly onto the substrate [3,20,21].

2. Experimental procedure

$(CuO)_{1-x}(ZnO)_x$ thin films were prepared onto chemically cleaned microscopy glass substrates by pneumatic spray pyrolysis technique from copper (II) chloride dihydrate and zinc acetate dihydrate dissolved in doubly distilled water. Different values of the nominal fraction of Zn, defined by x = Zn/(Cu+Zn) (with x = 0, 0.25, 0.50, 0.75 and 1), were used and controlled by changing the

solution concentration of the zinc and copper precursor source separately. The experimental setup described in previous works was adopted [1,22]. Solution concentration, nozzle-substrate distance, substrate temperature and spraying flow rate were kept constant during the whole deposition process at 0.025 mol/l, 30 cm, 450 °C and 9 ml/min, respectively. Comprehensive reaction process can be expressed as heat decomposition of copper (II) chloride dihydrate and/or zinc acetate dihydrate to clusters of CuO and/or ZnO in the presence of air oxygen and water [20,22].

Well adherent and transparent $(CuO)_{1-x}(ZnO)_x$ films were obtained. Surface roughness was checked and the film thickness was measured with a surface profilometer (Dektak 3st), keeping an estimated deposition time to obtain the same thickness of the films (~0.2 μm). The film structure was investigated by X-ray diffraction (XRD) with a scanning angle 2θ ranged between 20° and 80° using Philips X'Pert system operating at room temperature, 40 mA and 40 kV with a filtered Cu:K_α radiation (λ=1.5418 Å). The films optical transmittance was recorded in the wavelength range from 300 to 1500 nm using a SHIMADZU UV 3101 double-beam spectrophotometer. The electrical conductivity of $(CuO)_{1-x}(ZnO)_x$ thin films was measured by two-point probe using two gold electrodes stripes, deposited 2 mm apart on the film.

3. Results and discussion

3.1. Structural properties

Fig. 1 presents the recorded X-ray diffraction patterns of undoped CuO and undoped ZnO films prepared onto glass substrates by spray pyrolysis technique with two substrate temperatures 400 and 450 °C. As can be seen, the CuO film structure is improved with increasing substrate temperature, according to the noticeable increase in intensity of the two peaks located at 35.66° and 38.84° assigned to the (002) and (111) planes, respectively [2,23] according the JPCDS 45-0937. The structure of ZnO thin film is not altered by the substrate temperature at 400°C or 450°C [1].

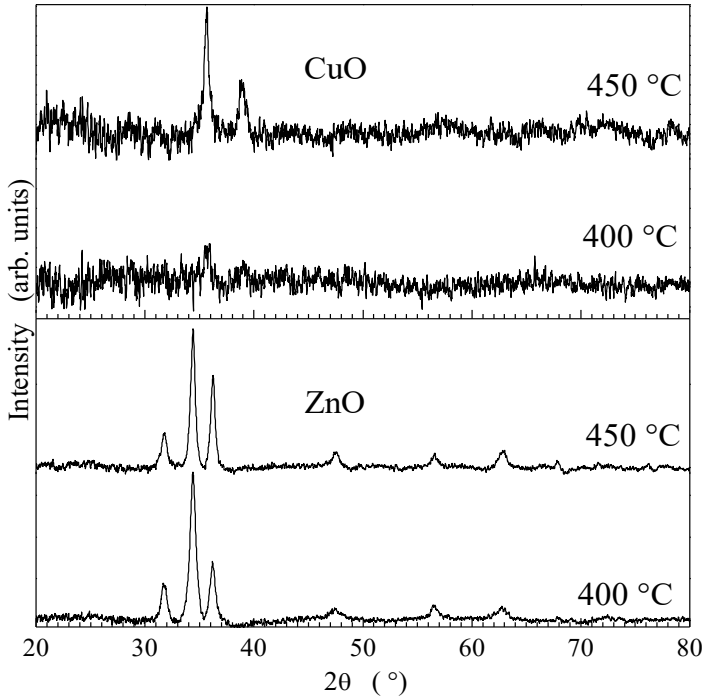

Fig. 1. X-ray diffractograms of CuO and ZnO films prepared at different substrate temperatures

The increase in intensity of the two peaks with increasing substrate temperature of CuO films was observed by Jhansi et al. [3]. It should be noted that this increase in intensity of the two peaks was also observed with increasing annealing temperature even if the copper oxide thin films were prepared by another deposition technique [23,24]. The increase in intensity of the two peaks which is accompanied by a decrease in full width at half maximum (FWHM) is due to the increase of the crystallite's sizes. This can be explained by the fact that the decrease of copper and/or oxygen defects are favorable to a merging process to form larger CuO grains when the substrate temperature is increased, which indicates the improvement of crystallinity of the CuO thin films due to gaining enough energy by the crystallites to orient in proper [4,7,23]. According to this, the substrate temperature in this work was fixed at 450 °C in the following.

Fig. 2 shows the XRD pattern of $(CuO)_{1-x}(ZnO)_x$ thin films deposited by spray pyrolysis at 450 °C on amorphous glass substrates for different *x* values.

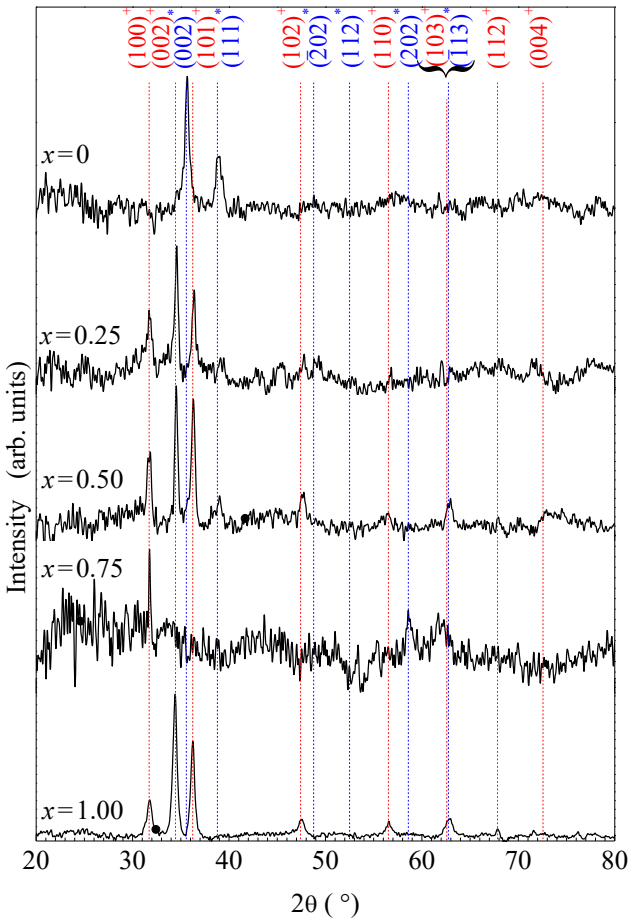

Fig. 2. XRD patterns of $(CuO)_{1-x}(ZnO)_x$ thin films deposited on the amorphous glass substrates at 450 °C and 0.025 M for different x values. $(hkl)^*$ for CuO and $(hkl)^+$ for ZnO (colour online)

The diffraction patterns indicate that the deposits have a polycrystalline structure. At $x = 0$, only the CuO peaks of monoclinic tenorite phase are observed (JCPDS: 41-0254) without the presence of metallic Cu (JCPDS: 04-0836) [25], Cu_2O (JCPDS: 05-0667) [25-27], or $Cu(OH)_2$ (JCPDS: 13-0420)[28]. At $x = 1$, only the ZnO peaks of hexagonal phase (JCPDS: 36-1451) are present [29,30] with a relatively high intensity compared to the CuO peaks [11]. For $x = 0.25$, 0.50 and 0.75, the presence of both CuO and ZnO peaks indicates the formation of CuO and ZnO phases mixed in defined proportions, the relative intensity of the (111) peak decreases with the complete disappearance of the (002) peak belonging to the CuO phase when the nominal fraction of Zn is increased, a slight shift of the diffraction peaks of CuO to lower 2θ values and the diffraction peaks of ZnO to higher 2θ values was clearly observed. These shifts in the diffraction peak positions can be ascribed to the substitution of Cu^{2+} by Zn^{2+} ions. No zinc or copper peak was observed in any of the diffractograms due to the substitution of lattice sites between zinc atoms and copper atoms due to the small difference in the ionic radius of Cu^{2+} (0.73 Å) and Zn^{2+} (0.74 Å) manifests that Zn^{2+} easily substitute Cu^{2+} [10,16]. It was also observed that all peaks of the zinc oxide phase are present with their preferred orientation varying. The stronger intensity of the diffraction peaks of ZnO compared to CuO indicates that the phase is more organized in ZnO [31]. This observation is similar to the results obtained by other authors with significant variations in diffraction intensity and angles [9-11]. Furthermore, as zinc concentrations increased, no solid solution formed between ZnO and CuO and no other peaks or significant shifts were observed.

Fig. 3 shows the evolution of average grain size versus the nominal fraction x in $(CuO)_{1-x}(ZnO)_x$ deposited at 450 °C and 0.025 M. The average crystallite sizes (D) of CuO and ZnO for each sample was determined from the XRD pattern using Scherrer equation (Eq. 1) [1]:

$$D = \frac{K\,\lambda}{\beta.\cos\theta} \tag{1}$$

where, K is the Scherrer's constant with a typical value of about 0.9, λ is the wavelength of X-ray used, β is the full width half maximum, and θ is the Bragg's diffraction angle [11].

The crystallite size was calculated using the peak (002) of each phase.

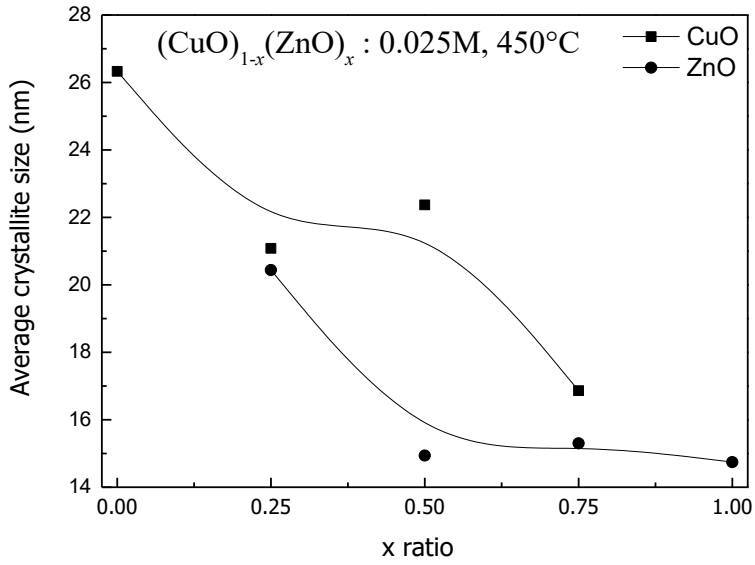

Fig. 3. Evolution of average crystallite size versus the nominal fraction x in $(CuO)_{1-x}(ZnO)_x$ deposited at 450 °C and 0.025 M

It can be noted that the crystallite size of undoped CuO ($x = 0$) has a significant value and is larger than the other of the crystallite sizes of undoped ZnO ($x = 1$) and the crystallite size of ZnO and CuO in mixture compound. This is what made the choice of experimental conditions for preparing the all samples (T = 450 °C) as shown in the Fig. 1. In addition to that, the crystallite size of ZnO and CuO in the mixture compound decreases when the nominal fraction of Zn increases in the initial solution which is explained by the difference in formation energy between ZnO and CuO. The enthalpy of formation of ZnO (ΔH_f = -350.9 kJ/mol) is lower than that of CuO (ΔH_f = -156 kJ/mol), the formation of ZnO is more favorable than the CuO formation which affects the increase in its crystallite size [1].

For $x = 0$, from (112), $(\bar{1}13)$, (002) and (200) reflection peaks, the lattice parameters for phase monoclinic CuO structure were calculated using the Eq. 2 [8,12,32]:

$$\frac{1}{d_{hkl}^2} = \frac{1}{sin^2\beta}\left(\frac{h^2}{a_{CuO}^2} + \frac{k^2 \sin^2\beta}{b_{CuO}^2} + \frac{l^2}{c_{CuO}^2} - \frac{2hl\ \cos\beta}{a_{CuO}c_{CuO}}\right) \quad (2)$$

where the interplanar spacing " d_{hkl} " was determined from the Bragg's law (Eq. 3) [3,13]:

$$2d_{hkl}\ sin\ \theta_{hkl} = \lambda \quad (3)$$

It was found that the values of their lattice constants (a_{CuO} = 4.65566 Å, b_{CuO} = 3.24344 Å, c_{CuO} = 4.99741 Å and β = 83.3675°) are lower than those of copper oxide nanoparticles powder values (a_{CuO} = 4.684 Å, b_{CuO} = 3.425 Å, c_{CuO} = 5.129 Å and β = 99.47°). This difference is due to the presence of compressive stress, a negative value was obtained for the strain (-2.56 %), resulting from the deposition conditions and attributed to the grain boundaries due to the difference in crystalline size. The strain is directly proportional to the lattice constant c_{XRD} and its value is related to the shift from the JCPDS standard value (c_{JCPDS}), it can be determined using the Eq. 4 [33]:

$$\text{Strain} = \left|\frac{c_{XRD} - c_{JCPDS}}{c_{JCPDS}}\right| \quad (4)$$

Considering the d_{hkl} paramater of the CuO and ZnO calculated from Eq. 3, it is evident that the CuO lattice expands with an increase in the Zn concentration in the sol while the ZnO lattice expands with an increase in the Cu concentration (decrease in Zn concentration). Both trends are likely explained by doping of the two oxide phases. An increasing Zn content in the sol leads to an increase in Zn-doping of the CuO structure and at the same time an increasing Cu content in the sol creates further Cu-doping of the ZnO structure [13]. While it is true that the Cu^{2+} and Zn^{2+} ionic radii have nearly the same size, significant doping may still lead to lattice constant expansion from other dopant occupation sites besides simple substitution such as interstitials and antisites (Fig. 3). An increase in native defect concentrations resulting from a high level of doping may also contribute to the lattice constant expansion [12].

The lattice parameters (a_{ZnO} and c_{ZnO}) for hexagonal phase of ZnO structure (Fig. 4) were calculated using the Eq. 3 and Eq. 5 [1,12,13]:

$$\frac{1}{d_{hkl}^2} = \frac{4}{3}\left(\frac{h^2+k^2+hk}{a_{ZnO}^2}\right) + \frac{l^2}{c_{ZnO}^2} \quad (5)$$

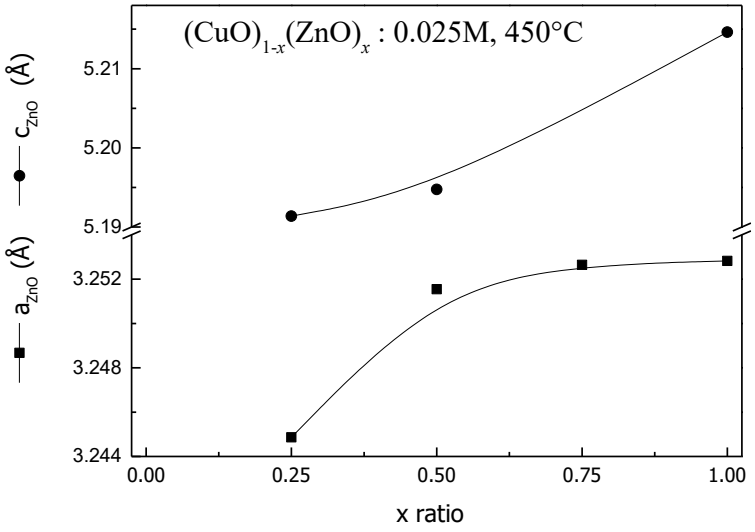

Fig. 4. Evolution of lattice constants of ZnO versus the nominal fraction x in $(CuO)_{1-x}(ZnO)_x$ deposited at 450 °C and 0.025 M

The slight increase in the lattice parameters of the ZnO component from the reported standard values, giving a clue that the two metal oxides (CuO and ZnO) unite together primarily through intra-grain coupling rather than inter-grain coupling [14,21].

3.2. Optical properties

Spectral optical transmittance of $(CuO)_{1-x}(ZnO)_x$ films deposited by spray pyrolysis technique onto glass substrates at 450 °C and 0.025 M are shown in Fig. 5. The front edges of the curves represent the intrinsic absorption [1,10]. The higher x value, the greater the optical transparency of films in the Visible-NIR region due to increased Zn content in the sol due to a higher relative content of ZnO in the $(CuO)_{1-x}(ZnO)_x$ films and the wide band gap of ZnO as compared to CuO [12]. Similar increase in the transmittance is due to decreasing irregular grains on the surface of CuO [12,34]. Also, the surface roughness of the CuO film would also contribute to the reduction of optical transparency through optical scattering [12,35,36].

Each spectrum can be divided into three regions according to wavelength (UV, Vis, and NIR). In the NIR, the obtained films exhibit high transparency (60-80%). In the visible, the optical transmission of the CuO films ($x = 0$) decreases when the wavelength decreases with interference fringes are not observed, this can be explained by the surface roughness of the thin films and the oxygen deficiency in the material resulting from its black color unlike ZnO ($x = 1$) which is more stoichiometric than the rest of the prepared films [10,37,38]. In the UV region (Fig. 5), the probability of electron transitions from the valence band to conduction band is directly allowed in zinc oxide, this is demonstrated by the sharpness of the optical absorption edge compared to alloys that contain the both of Cu and Zn ($0 < x < 1$) [36].

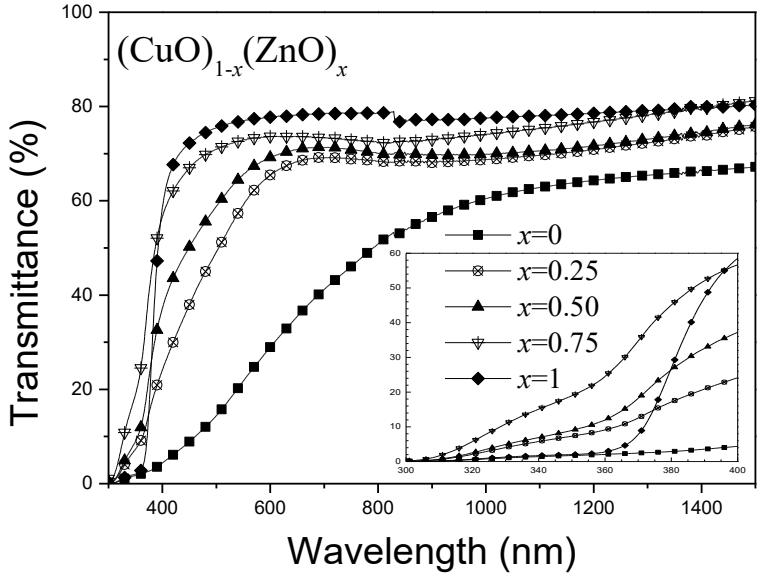

Fig. 5. Spectral variation of optical transmittance for $(CuO)_{1-x}(ZnO)_x$ films deposited at 450 °C and 0.025 M for different x values

From these spectra, the optical absorption coefficient (α) of the film of a thickness (d) is deduced as a function of absorbed light energy ($h\upsilon$) from the measured transmittance (T) using Beer–Lambert law [1,22,38]:

$$\alpha = \frac{1}{d}\ln\left(\frac{1}{T}\right) \quad (6)$$

The optical gap energy values (E_g)and the Urbach energy parameter (E_{Urb}) were deduced from the variations of the absorption coefficient with the photon energy ($h\upsilon$) using Tauc's formula for direct band semiconductors (Eq. 7) and Urbach's formula (Eq. 8), respectively [38]:

$$(\alpha h\upsilon)^2 = A\left(h\upsilon - E_g\right) \quad (7)$$

$$\ln\alpha = \left(\frac{1}{E_{Urb}}\right) h\upsilon + \ln\alpha_0 \quad (8)$$

where A and α_0 are constants, h is the Planck's constant, $h\upsilon$ is the photon light energy [16,35].

Fig. 6 shows the variation of the optical band gap energy and Urbach energy of $(CuO)_{1-x}(ZnO)_x$ films as a function of the nominal fraction x.

E_g values found are located between 2.8 eV for CuO (x = 0) and 3.3 eV for ZnO (x = 1). The increase in the band gap energy may be due to the sp–d spin-exchange interactions between the band electrons and the localized d electrons of the metal ion (Zn) substituting the Cu ion, the localization behavior of the zinc ions in the lattice planes leads to an increase of the hopping path of charge carriers and thus an increase of the band gap energy [13,15,39]. The highest value of Urbach energy (E_{Urb}) at 0 *at*. % Zn-doping concentration (Undoped CuO) can also be confirmed which has a narrow bandgap because of closely matching energy levels of 3d and 2p bands of Cu dopant and O atoms which lead to the exchange interaction between these bands [14]. Whereas, the defect density decreases drastically with the Zn is mixed in CuO host lattice in addition to the presence of the zinc oxide phase which is more stoichiometry [14]. Also, Ganesh et al. observed an inverse relationship between E_g and E_{Urb} on Cu-doped ZnO thin films [16].

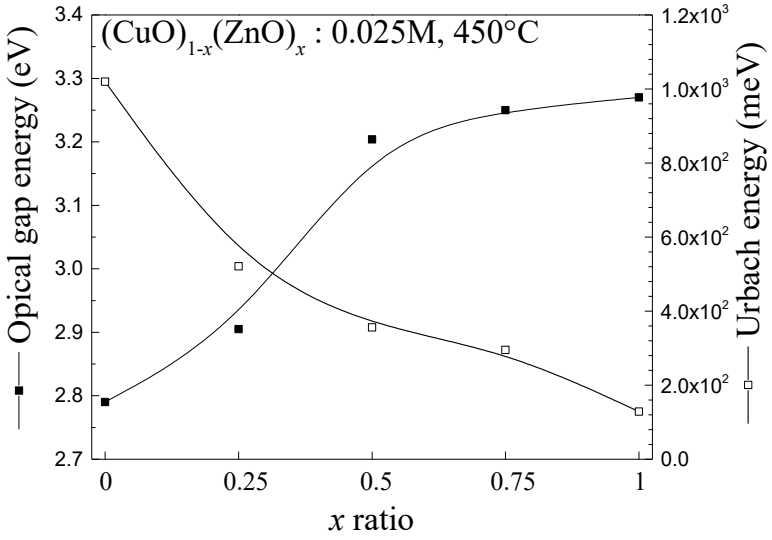

Fig. 6. Variation of optical gap and Urbach energy versus the nominal fraction x in $(CuO)_{1-x}(ZnO)_x$ films deposited at 450 °C and 0.025 M

3.3. Electrical conductivity

The dark electrical conductivity of the $(CuO)_{1-x}(ZnO)_x$ films was measured using the conventional two-point probe. The current–voltage characteristics revealed a linear relation indicating an ohmicity of the electrical contacts [13,40]. Fig. 7 shows the variation of the electrical conductivity (σ) of $(CuO)_{1-x}(ZnO)_x$ samples formed at different x values. As can be seen, the conductivity increases noticeably with increasing the nominal fraction of Zn, the zinc ions are no longer able to occupy more Cu sites and as segregation of Zn ions intra-grain of CuO or interstices resulting in the formation of a zinc oxide phase [13].

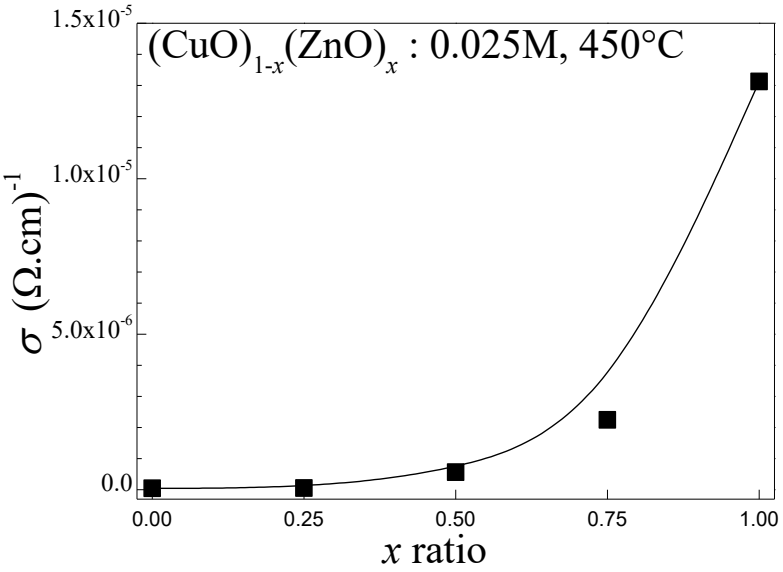

Fig. 7. Variation of electrical conductivity versus the nominal fraction x in $(CuO)_{1-x}(ZnO)_x$ films deposited at 450 °C and 0.025 M

On the one hand, the CuO is a p-type material and has a low electrical conductivity [17], while ZnO is an n-type and has a high electrical conductivity due to the difference in electron and hole mobilities [13,17]. On the other hand, Khalfallah et al. have found that there is a direct relationship between the optical gap energy and the electrical conductivity of zinc oxide doped with different percentages of copper [15]. The conductivity type of the deposited $(CuO)_{1-x}(ZnO)_x$ films can be controlled by simply varying the nominal fraction x. The conductivity evolves then from p-type with $x = 0$ towards n-type for $x = 1$.

4. Conclusions

$(CuO)_{1-x}(ZnO)_x$ films have been prepared by pneumatic spray pyrolysis technique on glass substrates from copper (II) chloride dihydrate and zinc acetate dihydrate solutions at 0.025 mol/l and 450 °C. The obtained results indicate that the prepared films were adhering well onto glass substrate, have surface roughness and their properties can be controlled through the nominal fraction x of Zn. The XRD patterns indicate that the films are polycrystalline and show the presence of only one phase of CuO or ZnO when $x = 0$ or 1, respectively. For intermediate compositions ($x = 0.25$, 0.50 and 0.75), the $(CuO)_{1-x}(ZnO)_x$ films are composed of two phases mixed in defined proportions. The optical gap energy and electrical conductivity increase with the nominal fraction of Zn.

References

[1] L. Herissi, L. Hadjeris, M. S. Aida, J. Bougdira, Thin Solid Films **605**, 116 (2016).
[2] A. M. Mansoor Al-Saeedi, F. Mohamad, N. Ridha, Journal of Nanostructures **12**, 686 (2022).
[3] N. Jhansi, D. Balasubramanian, J. H. Chang, K. Mohanraj, R. Marnadu, M. A. Manthrammel, M. Shkir, Silicon **14**, 8193 (2022).
[4] S. S. Roy, A. H. Bhuiyan, J. Podder, Sensors and Transducers **191**, 21 (2015).
[5] K. C. Sanal, L. S. Vikas, M. K. Jayaraj, Applied Surface Science **297**, 153 (2014).
[6] M. Asadi, S. M. Rozati, Materials Science-Poland **35**, 355 (2017).
[7] A. A. Ejigu, Physica Scripta **97**, 115005 (2022).
[8] R. Daira, B. Boudjema, A. Mohammedi, Chalcogenide Letters **20**, 277 (2023).
[9] J. O. Adeyemi, D. C. Onwudiwe, A. O. Oyedeji, Molecules **27**, 3206 (2022).
[10] A. Alsulmi, N. N. Mohammed, A. Soltan, M. F. Abdel Messih, M. A. Ahmed, RSC Advances **13**, 13269 (2023).
[11] P. Sable, N. Thabet, J. Yaseen, G. Dharne, Trends in Sciences **19**, 3092 (2022).
[12] Y. Caglar, D. D. Oral, M. Caglar, S. Ilican, M. A. Thomas, K. Wu, Z. Sun, J. Cui, Thin Solid Films **520**, 6642 (2012).
[13] H. A. Al-Khanbashi, W. Shirbeeny, A. A. Al-Ghamdi, L. M. Bronstein, W. E. Mahmoud, Ceramics International **40**,1927 (2014).
[14] K. Joshi, M. Rawat, S. K. Gautam, R. G. Singh, R. C. Ramola, F. Singh, Journal of Alloys and Compounds **680**, 252 (2016).
[15] B. Khalfallah, I. Riahi, F. Chaabouni, Optical and Quantum Electronics **53**,238 (2021).
[16] V. Ganesh, G. F. Salem, I. S. Yahia, F. Yakuphanoglu, Journal of Electronic Materials **47**, 1798 (2017).
[17] F. Ye, X-Q. Su, X.-M. Cai, Z.-H. Zheng, G.-X. Liang, D.-P. Zhang, J.-T. Luo, P. Fan, Thin Solid Films **603**, 395 (2016).
[18] C. A. Canbay, A. Aydogdu, Turkish Journal of Science andTechnology **4**, 121 (2009).
[19] C. H. Kwon, H. K. Hong, D. H. Yun, K. Lee,

S. T. Kim, Y. H. Roh, B. H. Lee, Sensors and Actuators B: Chemical **25**,610 (1995).
[20] L. Hadjeris, L. Herissi, M. Benbouzid, N. Attaf, M. B. Assouar, T. Easwarakhanthan, M. S. Aida, J. Bougdira, A. Mahdjoub, Algerian Journal of Advanced Materials **4**, 9 (2008).
[21] S. Abu Bakar, S. T. Hussain, S. A. Trimizi, M. N. Tahir, Polyhedron **49**, 138 (2013).
[22] L. Hadjeris, L. Herissi, M. B. Assouar, T. Easwarakhanthan, J. Bougdira, N. Attaf, M. S. Aida, Semiconductor Science and Technology **24**, 035006 (2009).
[23] A. Bougharouat, N. Touka, D. Talbi, K. Baddari, Annales de Chimie-Science des Matériaux **45**, 439 (2021).
[24] M. Abdel Rafea, N. Roushdy, Journal of Physics D: Applied Physics **42**, 015413 (2009).
[25] F. Du, J. Liu, Z. Guo, Materials Research Bulletin **44**, 25 (2009).
[26] U. C. Bind, R. K. Dutta, G. K. Sekhon, K. L. Yadav, J. B. M. Krishna, R. Menon, P. Y. Nabhiraj, Superlattices and Microstructures **84**, 24 (2015).
[27] J. Wang, L. Li, D. Xiong, R. Wang, D. Zhao, C. Min, Y. Yu, L. Ma, Nanotechnology **18**, 075705 (2007).
[28] M. Qiu, N. Wang, Z. Cui, J. Liu, L. Hou, J. Liu, R. Hu, H. Zhang, Y. Zhao, Journal of Materials Chemistry A **6**, 817 (2018).
[29] S. A. Rane, S. M. Pudi, P. Biswas, Chemical and Biochemical Engineering Quarterly **30**, 33 (2016).
[30] M. García-Hipólito, C. D. Hernández-Pérez, O. Alvarez-Fregoso, E. Martínez, J. Guzmán-Mendoza, C. Falcony, Optical Materials **22**, 345 (2003).
[31] K. Yu, Y. Zhang, L. Luo, S. Ouyang, H. Geng, Z. Zhu, Materials Letters **59**, 3525 (2005).
[32] H. Z. Asl, S. M. Rozati, Materials Research **21**, e20170754 (2018).
[33] A. H. O. Alkhayatt, S. K. Muhammad, A. A. Habieb, A. H. Ali, S. H. Mohsen, R. R. Munem, IOP Conf. Series: Materials Science and Engineering **871**, 012094 (2020).
[34] K. H. Yoon, W. J. Choi, D. H. Kang, Thin Solid Films **372**, 250 (2000).
[35] A. A. Ogwu, E. Bouquerel, O. Ademosu, S. Moh, E. Crossan, F. Placido, Acta Materialia **53**, 5151 (2005).
[36] G. K. Mani, J. B. B. Rayappan, Journal of Alloys and Compounds **582**, 414 (2014).
[37] S. S. Shinde, P. S. Patil, R. S. Gaikwad, R. S. Mane, B. N. Pawar, K. Y. Rajpure, Journal of Alloys and Compounds **503**, 416 (2010).
[38] L. Herissi, L. Hadjeris, M. S. Aida, S. Azizi, A. Hafdallah, A. Ferdi, Nano Hybrids and Composites **27**, 21 (2019).
[39] R. Elilarassi, G. Chandrasekaran, Journal of Materials Science: Materials in Electronics **21**, 1168 (2010).
[40] S. J. Ikhmayies, N. M. Abu El-Haija, R. N. Ahmad-Bitar, Journal of Semiconductors **36**, 033005 (2015).

*Corresponding author: labidi.herissi@univ-tebessa.dz